JAMI
Journal of Applied Mathematics and Informatics

J. Appl. Math. & Informatics Vol. **44***(2026), No. 5, pp. 2019 - 2042*
https://doi.org/10.14317/jami.2026.2019

VARIATIONAL OPTIMIZATION AND HYBRID IMAGE INPAINTING USING TOPOLOGICAL EXEMPLAR AND HIGH-ORDER DIFFUSION TECHNIQUES

AHMED K. AL-JABERI, ZAINAB H. AHMED AND ALI HASAN ALI*

Abstract. The process of reconstructing missing or deteriorated regions in digital images has evolved significantly from traditional manual restoration to sophisticated computational approaches known as image inpainting. This paper examines the development of hybrid image inpainting techniques that combine multiple methodologies to overcome the limitations of individual approaches. A novel merged restoration (NMR) technique that combines a Topological Exemplar-Based Inpainting (TEBI) method to reconstruct the damaged region's texture component with a high-order diffusion equation (H-ODE) algorithm to reconstruct the damaged area's structure component is improved. The outcomes of applying the hybrid inpainting approach for reconstructing damaged areas are promising, as both the high-order diffusion and the TEBI methods have successfully recovered missing areas with high structure and texture in the surrounding areas. Statistical image quality measures have been utilized to assess the performance of the hybrid technique and study its effectiveness. Several experimental studies are applied to clarify the extent of the hybrid technique, though their results are compared with those obtained using the high-order diffusion equation and the TEBI method.

AMS Mathematics Subject Classification : 68U10, 65D18, 49M25.
Key words and phrases : Image inpainting, hybrid image restoration, high-order diffusion equation, numerical optimization, variational optimization.

1. Introduction

Image inpainting, also known as image completion, is a fundamental problem in computer vision and image processing that involves reconstructing missing

Received June 20, 2026. Revised August 10, 2026. Accepted August 25, 2026. *Corresponding author.
© 2026 KSCAM.

or degraded parts of an image. The primary objective is to fill missing regions—typically defined by a binary mask—with plausible, semantically coherent, and visually seamless content, rendering the restored area indistinguishable from the surrounding image. This technique has found extensive applications across diverse domains, including the restoration of historical photographs and artworks, object removal in photo editing, privacy protection through content concealment, and completion of corrupted medical imagery.

This paper reviews the trajectory from traditional methods to current state-of-the-art approaches, with a specific focus on the motivation, development, and recent advancements in hybrid models [1]. The foundation of image inpainting research rests upon two primary methodological schools: diffusion-based and exemplar-based approaches, each with distinct operational principles and application domains.

Diffusion-based (or structure-based) methods, pioneered by Bertalmio et al. in [2], spread information from the boundary of the damaged area inward. This propagation is typically guided by partial differential equations (PDEs) [3], or variational principles [4], effectively "smoothing" known information into target areas. The total variation (TV) model represents a classic example of this approach. The fundamental strength of diffusion-based methods lies in their exceptional ability to reconstruct thin structures, sharp edges, and small gaps, ensuring geometric continuity.

Exemplar-based (or texture-based) methods, popularized by Efros and Leung in [5] and later refined by Criminisi et al. in [6], adopt a fundamentally different strategy. These techniques fill target regions by searching for similar patches (exemplars) in the known portions of the image and copying them into the target regions. The fill order is typically determined by a priority function that favors patches lying on strong structures, aiming to preserve line continuity into the filled area. These methods [7] excel in the synthesis of repetitive textures and are suitable for larger missing regions, provided that suitable source patches are available.

Recognizing that natural images require combined approaches. Early hybrid methods emerged as direct responses to the complementary weaknesses of diffusion- and exemplar-based techniques. These pioneering hybrid models often decomposed images into two layers: a structure layer containing edges and smooth regions, and a texture layer containing detailed patterns [8]. The structure layer would be inpainted using diffusion-based methods. In contrast, the texture layer would be synthesized using exemplar-based methods and the final results would be obtained by combining the two inpainted layers [9].

The advent of deep learning, particularly Convolutional Neural Networks (CNNs) [10] and Generative Adversarial Networks (GANs) [11], marked a paradigm shift in inpainting research. Unlike traditional approaches that rely on low-level pixel propagation or patch matching, these data-driven methods learn to understand high-level semantics and generate contextually appropriate novel content. GANs became particularly dominant, with models such as the Context

Encoder proposed by Pathak et al. in [12] using adversarial training to produce visually plausible completions of large missing regions. Subsequent advances incorporated global and local discriminators to balance semantic accuracy and realism of detail.

The deep learning era has given rise to a contemporary interpretation of hybrid techniques: integrating multiple deep learning components with each other or with traditional algorithms to create more robust and effective systems. CNN-Transformer Hybrid Architectures [13] represent a prominent direction in modern hybrid inpainting. While CNNs [14] excel at capturing local textures and edges through their inductive biases, Transformers leverage self-attention mechanisms to model long-range dependencies and global semantic structures. Recent models have proposed multi-branch parallel [15] architectures in which CNN branches capture fine-grained local features. In contrast, the transformer branches model global context, with dynamic fusion mechanisms that adaptively combine multi-scale features based on the characteristics of missing regions.

The integration of classical algorithms with Deep Learning [16] has also emerged as a powerful hybrid strategy. For example, the DKH method explicitly combines three distinct phases: a Deep CNN for residual image generation, K-Nearest Neighbors (KNN) for patch-based reconstruction (descending from exemplar-based methods), and biH-ODE functions (PDE-based diffusion techniques) for medical image reconstruction, with final outputs created through Bayesian probabilistic-based fusion [17].

Mamba-Transformer Hybrids [18] represent the cutting edge of hybrid architecture design. Recent work has introduced MxT (Mamba x Transformer), which combines Mamba's efficiency in processing long sequences with linear computational cost with the Transformer's capacity for understanding global interactions. This hybrid facilitates dual-level interaction learning at both pixel and patch levels, significantly enhancing reconstruction quality and contextual accuracy.

Integrating a diffusion model [19] represents another frontier in hybrid inpainting. Diffusion models generate images through iterative denoising processes, gradually removing Gaussian noise to reveal meaningful structures. Wavelet-based diffusion models (WaveDM) have demonstrated state-of-the-art performance with efficiency comparable to traditional one-pass methods while being more than $100\times$ faster than vanilla diffusion models.

Wavelet-based hybrid methods [20] have shown particular promise for maintaining structural continuity. Recent frameworks combine diffusion models, such as the Cahn-Hilliard model, with wavelet transforms to decompose images into distinct frequency components, enabling targeted processing of different frequency bands. LaMa-Wavelet networks [21] similarly apply wavelet transforms within the architecture to improve the reconstruction of image edges and fine details, especially with large masks.

This paper proposes a Novel merged restoration (NMR) method to recover various types of missing regions in images across different color spaces. The

NMR method was proposed by combining the TEBI method [23] and the H-ODE algorithm [22], enabling this method to recover large missing regions while preserving edges and corners without artifacts in an image. The rest of the paper is introduced as follows: Section 2 introduces the research methodology for image inpainting, including the image decomposition method, the H-ODE algorithm, and the TEBI method. Section 3 presents the NMR method for simultaneously reconstructing texture and structural regions missing from color images. Section 4 presents numerical results for applying the proposed technique and other methods for recovering missing regions in an image across different color spaces. Finally, the outcomes and upcoming work are given in Section 5.

2. Research Methodology

This section presents the components used in the proposed NMR technique. This work introduces the image decomposition method, the H-ODE algorithm, and the TEBI method.

2.1. Image decomposition method.

The core principle underlying the splitting equation presented in this section is outlined below: The damaged image is divided into two components—a structural component and a texture component. If $I(x, y)$ represents the original damaged image, then $I(x, y) = w(x, y)+r(x, y)$, where $r(x, y)$ is the texture component, and $w(x, y)$ is the structural component. The goal is to create a cleaner version of the image while preserving the clarity of all important edges, smoothing out smooth areas, and separating the texture from any noise [24]. Each component is optimized using specialized techniques: the H-ODE and TEBI methods are used to recover the missing regions in the structure and texture components, respectively. After these steps, the two components are combined to produce the final reconstructed image. To reduce noise, the MTV method is used to separate the image into its basic texture and structure details. The MTV model [25] is applied to remove noise from the image by combining the advantages of Tikhonov TV-L^2 and Total Variation TV-L^1 methods. It can be formulated as the following minimization problem:

$$\min_{w\in BV(\Omega)} \left[\lambda\|f-w\|_{L^2}^2 + \alpha\|\nabla w\|_{L^1} + \frac{\beta}{2}\|\nabla w\|_{L^2}^2\right], \tag{1}$$

where $\lambda > 0$ represents a scaling parameter, α preserves and reconstructs information in high-texture detailed areas, and β controls noise removal in low-texture regions. To minimize this functional (1), the Euler–Lagrange equation is used, and then a gradient descent scheme is applied, leading to:

$$w_t = \lambda(f-w) + \alpha\nabla\cdot\frac{\nabla w}{\|\nabla w\|} + \beta\Delta w. \tag{2}$$

In this framework, the parameters β,α, and λ are carefully chosen to balance noise reduction with the preservation of important image characteristics, such as

edges and corners. This improved formula addresses some shortcomings of the traditional TV-L^1 and TV-L^2 models, yielding better overall results. Using this model, the image is separated into its structural and textural components. The equations are solved numerically using the finite difference method (FDM) [26]. To select appropriate parameter values, λ is studied experimentally. The setting $\lambda = 2$ was found to provide the best performance, while different values of β and α are tested, as clarified in Section 4.1.

2.2. Structural recovery via the high-order diffusion algorithm.

The Navier–Stokes equations [1] inspire the high-order diffusion algorithm. Isophotes [27] are transferred to the missing region with a propagation that maintains structural continuity (i.e., transfers information to the length of isophotes). Isophotes are lines where the intensity of the image is constant. This equation uses the transport equation to spread information through missing regions and the diffusion equation [22] to maintain numerical stability. This algorithm is widely used in image processing. Let $I(x, y)$ be a digital image that represents an intensity function, where I is a pixel intensity, x, y are the coordinates of the image, and the image is divided into two regions: Ω is the damaged region (inpainting region) and $\partial\Omega$ is the border of the missing region. The objective is to reconstruct the values in Ω from the information on the boundary $\partial\Omega$. The formula of the high-order diffusion equation (H-ODE) is given below:

$$I_t = \mu(\nabla^{\perp} I \cdot \nabla(\Delta I)) + \xi \Delta I \tag{3}$$

Where $\mu(\nabla^{\perp} I \cdot \nabla(\Delta I))$ is a transport term, μ is a transport parameter, $\nabla^{\perp} I = (-I_y, I_x)$ is isophotes, ΔI is the Laplacian of the image, $\xi \Delta I$ is the diffusion term and ξ is the diffusion parameter. Recover missing areas in RGB color images by applying equation (3) to each color channel (R, G, B) and then merging the results. Then, FDM [26] is applied to solve equation (3) for each channel of the color image. The basic idea of the suggested H-ODE model is based on:

- Transfer of edge information along isophote lines.
- Gradually fill in the missing region.

This is similar to the transfer of the vortex in fluids described by the Navier-Stokes equations, as shown in Figure 1.

Equation (3) is approximated using the finite differences method, as follows:

$$I_t(i, j) = \mu(\vec{N}_n(i, j) \cdot \delta L_n(i, j)) + \xi \Delta I_n(i, j) \tag{4}$$

The gradient of the image is $\nabla I(i, j) = (I_x, I_y)$, where $I_x = \frac{I^n(i+1,j) - I^n(i-1,j)}{h}$, $I_y = \frac{I^n(i,j+1) - I^n(i,j-1)}{k}$, the Laplacian of the image is $\Delta I = I_{xx} + I_{yy}$, then the finite difference for the Laplacian operator is:

$$\Delta I = \frac{I^n(i+1, j) - 2I^n(i, j) + I^n(i-1, j)}{h^2} + \frac{I^n(i, j+1) - 2I^n(i, j) + I^n(i, j-1)}{k^2}.$$

The isophote will be represented as $\vec{N} = \frac{(-I_y(i,j), I_x(i,j))}{\sqrt{I_x(i,j)^2 + I_y(i,j)^2}}$. The Laplace gradient for the image is $\nabla(\Delta I) = (L_x, L_y)$, where $L_x = \frac{\partial(\Delta I)}{\partial x}$, $L_y = \frac{\partial(\Delta I)}{\partial y}$.

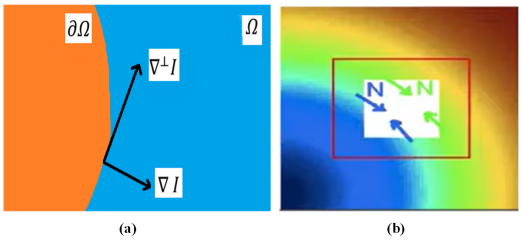


FIGURE 1. Explanation of the H-ODE algorithm. (a) Spreading direction by vertical normal operator to the border, (b) Spreading direction inward the damaged area.

The transport term is written as transport $= \nabla^{\perp} I \cdot \nabla(\Delta I)$, then transport $= (-I_y)L_x + (I_x)L_y$. Finally, the time Euler method is applied to update only inside the damaged area in equation (4) as follows:

$$I^{n+1}(i,j) = I^{n}(i,j) + \left(\mu\left(\vec{N}_n(i,j) \cdot \delta L_n(i,j)\right) + \xi \Delta I_n(i,j)\right)\Delta t \qquad (5)$$

Figure 2 illustrates a block diagram of the suggested H-ODE method.

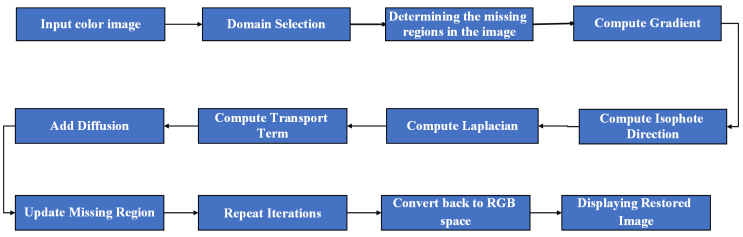


FIGURE 2. Flowchart of high-order diffusion (H-ODE) algorithm.

Figure 3 illustrates the restoration of missing areas using the H-ODE algorithm and the diffusion, transport and Mumford-Shah methods given in [1], [22], and [28], respectively.

The implementation of the H-ODE algorithm alongside other algorithms in 5000 iterations, such as diffusion, transport, and Mumford-Shah, as shown in [1], [22], and [28], respectively, is shown in Figure 3. In visual comparison, the H-ODE algorithm outperformed the other given methods. This H-ODE algorithm successfully reconstructed borders. It is a 3^{rd}-order PDE, used as given in Figure 3. In outline, curvature maintaining is not achieved in large areas of missing data by the methods given in [24], [23] and [22], but the H-ODE model successfully recovered them (the connectivity principle is satisfied).

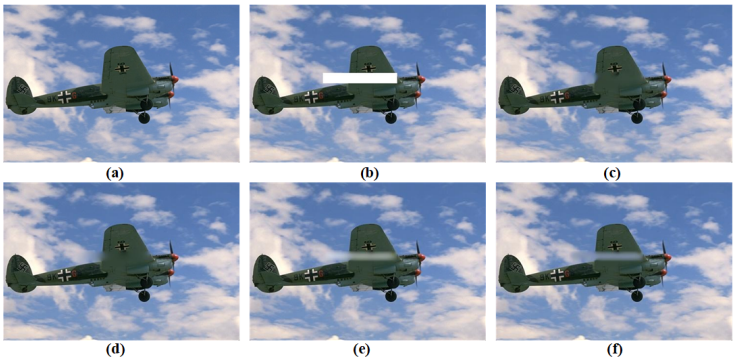


FIGURE 3. Object removal. (a) Reference image, (b) reference image with a mask, (c), (d), (e), and (f) reconstructed image via H-ODE algorithm and methods at 5000 iterations given in [1], [22], and [28], respectively.

2.3. Topological Exemplar-based Texture Synthesis.

The missing areas within the texture component are reconstructed using the Topological Exemplar-based Inpainting method (TEBI) [23]. This method relies on three main aspects: selecting an appropriate patch size, defining a priority function, and establishing a matching criterion. First, the patch size (i.e., the window used during the filling process) is specified based on its similarity to neighboring regions. This is achieved by analyzing the areas surrounding the damaged area using Topological Data Analysis (TDA). Specifically, the most suitable patch size for propagation is determined by computing connected components using local binary patterns [23]. Second, the method prioritizes candidate patches based on the curvature of the isoluminescence lines (i.e., isophotes). The priority function ($P(p)$) based both on the confidence term ($C(p)$) and the data term ($D(p)$) [29], which are known as follows:

$$P(p) = C_1 \times R_c(p) + C_2 \times D(p) + \|\nabla I_p\|^{-1/2} \tag{6}$$

where $R_c(p)$ is a regularization confidence term, which is given as

$$R_c(p) = (1-\varepsilon) \times C(p) + \varepsilon, \quad 0 < \varepsilon < 1 \tag{7}$$

and

$$C(p) = \frac{\sum_{q \in \psi_p \cap (I-\Omega)} C(q)}{\|\psi_p\|}.$$

The improved data term $D(p)$ is given as follows:

$$D(p) = \frac{\|\nabla I_p^{\perp} \cdot \mathbf{n}_p\|}{\alpha + \left\|\nabla \cdot \frac{\nabla I_p}{\|\nabla I_p\|}\right\|} \tag{8}$$

Where C_1 and C_2 are the weight elements, which were set in terms of the amount of texture in an image, inspired by the work of [30]. The ∇I is a gradient of the image I, $\nabla I_p^{\perp}$ is the isophote, intensity, and direction at point p, $\|\psi_p\|$ is the area of ψ_p, $\alpha = 255$ for a typical gray-level image, $\mathbf{n}_p$ is a unit vector orthogonal to the front $\partial\Omega$ in the point p and $\perp$ denotes the orthogonal operator. The parameter ε controls the fluency of the curves.

Third, applying matching criteria between the patches in two phases:

1- The sum of squared distances (SSD) measure is applied to patches in the spatial, Laplace, and gradient domains of an image, and the 40 patches with the lowest SSD value are selected (i.e., the closest patches).

$$d_G(G(\psi_p), G(\psi_q)) = \{\|\psi_x(p) - \psi_x(q)\| \ \& \ \|\psi_y(p) - \psi_y(q)\| < t\}, \tag{9}$$

The $d_G(G(\psi_p), G(\psi_q))$ is an SSD value that is calculated using the L^2-norm distance as above; t is a threshold value for partial derivatives of the image I in the x and y directions.

$$\psi_q^* = \arg\min_{\psi_p \in \Omega} d_s(I(\psi_p), I(\psi_q)) + d_g(G(\psi_p), G(\psi_q)) + d_l(L(\psi_p), L(\psi_q)) \tag{10}$$

where ψ_p and ψ_q are sample and candidate patches, respectively. d_s, d_g, and d_l are the distances between the sample and the candidate patches in the spatial, gradient, and Laplacian image, respectively.

2- The Normalized Correlation Coefficient (NCC) is applied to the 40 patches. The NCC between the template is calculated, and the 40 nearest candidate patches are specified to find the patch with the NCC value closest to 1. The NCC formula is given as [40]:

$$d_{NCC}(I(\psi_p), I(\psi_q)) = \frac{\sum(\psi_p) \cdot (\psi_q)}{\sqrt{\sum(\psi_p)^2}\sqrt{\sum(\psi_q)^2}} \tag{11}$$

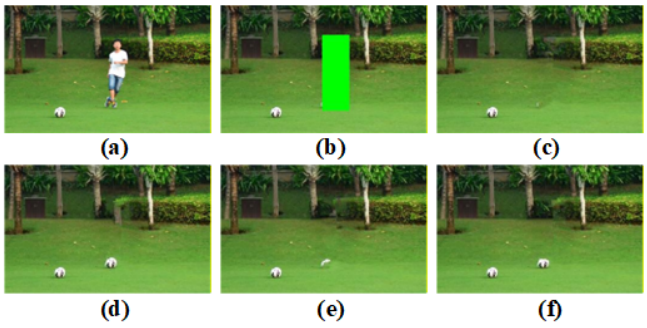


FIGURE 4. Object removal. (a) Reference image, (b) reference image with a mask, (c), (d), (e), and (f) reconstructed image via the TEBI method [23] and methods given in [31], [32], and [33], respectively.

Figure 4 illustrates the removal of objects using the TEBI method and the methods given in [31], [32], and [33].

Figure 4 clarifies the implementation of the TEBI method alongside different algorithms, such as [31], [32], and [33]. In visual comparison, the TEBI method outperformed the other given methods.

3. Novel merged restoration technique for a color image

After applying the MTV method, the image is decomposed into two components: texture and structure. Each component is then restored separately in the damaged regions using appropriate inpainting techniques. The NMR approach reconstructs both structural and textural parts simultaneously. Specifically, it uses the TEBI method to recover one component and the H-ODE model to restore the other. Finally, the reconstructed texture and structure are combined to produce the final image. This process is applied in eight different color spaces. Figure 5 illustrates the block diagram of the proposed NMR method.

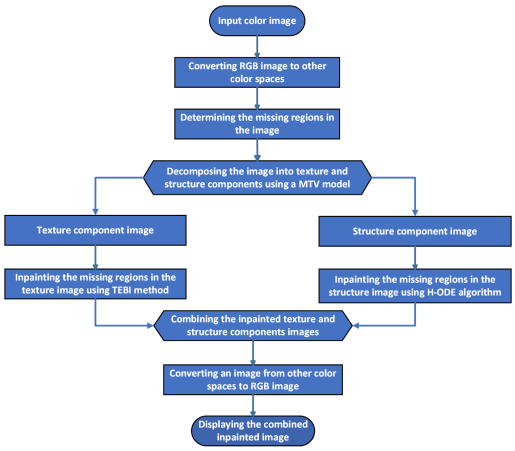


FIGURE 5. Flowchart of the NMR technique for image inpainting.

The experimental results are presented to evaluate the effectiveness of the proposed NMR technique and then compare them with results obtained from the TEBI [23] and H-ODE methods.

4. Experimental implementation

The suggested MTV model was numerically implemented and solved using the FDM method [26] on 100 color images from the Berkeley database [34], which include low- and high-texture images, as illustrated in Figure 6. These images were chosen for their level of structure and texture, which supports evaluating the effectiveness of the NMR technique in restoring missing areas.



FIGURE 6. Example of ten out of 100 color images.

The performance of the NMR method was assessed by comparing its results with those obtained from the H-ODE model and the TEBI approach using statistical quality measures (SQMs). These SQMs are computed between the inpainted and original images and include mean squared error (MSE), peak signal-to-noise ratio (PSNR) [35], structural similarity index (SSIM) [36, 37], and the entropy [38]. These quantitative metrics are used to assess image quality and should agree with the qualitative evaluation. In addition, the processing time required to produce the results was examined to evaluate the efficiency of the inpainting methods. The NMR algorithm was implemented in MATLAB (R2022a) and executed on a Huawei laptop equipped with an Intel Core i5-10210U processor and 8 GB of RAM. Experimental tests were conducted on images with large missing regions to evaluate the effectiveness and robustness of the proposed method.

4.1. Image Decomposition Experiments.

The MTV model decomposes an image into structure and texture components. In this study, the effects of α and β on the performance of the MTV model with removed image noise are investigated. This study was conducted on 100 color images, choosing different values of β and α. Salt-and-pepper noise was added to the images with 600 iterations. Table 1 summarises the mean values of MSE, SSIM, PSNR, entropy, and the time required to obtain results using the MTV model.

TABLE 1. SQMs for salt&pepper noise removal in images, iteration=600, obtained results using the MTV model at different values of parameters α and β.

Parameters	MSE	PSNR	SSIM	Entr(O)	Entr(I)	Time(s)
$\alpha = 0.05, \beta = 0.5$	18.20882	35.52799	0.65890	6.6831	6.19553	174.3483
$\alpha = 0.01, \beta = 1.0$	91.52383	28.51546	0.06258	6.6831	3.58672	581.2251
$\alpha = 0.1, \beta = 1.5$	68.89158	29.74914	0.33604	6.6831	4.41173	842.5166
$\alpha = 0.5, \beta = 0.05$	45.85381	31.51705	0.11213	6.6831	5.78059	315.5669
$\alpha = 1.0, \beta = 0.01$	30.02213	33.35639	0.00839	6.6831	5.83543	780.6931
$\alpha = 1.5, \beta = 0.1$	58.25459	30.47754	0.05945	6.6831	5.33640	58.65872
$\alpha = 0.05, \beta = 0.05$	25.67335	34.03598	0.03121	6.6831	5.80433	489.7951
$\alpha = 0.01, \beta = 0.01$	11.05548	37.69503	0.60326	6.6831	6.31816	265.4888
$\alpha = 0.5, \beta = 0.5$	20.50618	35.01196	0.30153	6.6831	6.04970	376.9036

The results of the MTV model were promising, as seen in Table 1. The results were stable, and the model's performance was good for the parameter values β and α. The MTV model is used to divide the image into structural and textural components, with parameter values α=0.01, β=0.01, and λ=2 used for 600 iterations.

4.2. Image inpainting experiments using the H-ODE method.

The H-ODE model is used to recover damaged regions in an image. In this study, the effects of the values μ and ξ on the performance of the H-ODE model to recover missing regions in an image are investigated. The values of μ and ξ are chosen differently, as shown in Table 2. This study was conducted on 100 color images. Table 2 summarises the mean values of MSE, SSIM, PSNR, entropy, and the time required to obtain results using the H-ODE model at different values of μ and ξ, with 900 iterations.

TABLE 2. SQMs for recovering missing regions in images, iteration=900, obtained results using the H-ODE model at different values of parameters μ and ξ.

Parameters	MSE	PSNR	SSIM	Entr(O)	Entr(I)	Time(s)
$\mu = 0.001, \xi = 0.01$	96.9073	28.2672	0.0600	6.6831	5.5946	21.4907
$\mu = 0.05, \xi = 0.5$	4.92295	41.2085	0.3250	6.6831	6.3554	28.4006
$\mu = 0.1, \xi = 0.05$	35.1441	32.6723	0.0992	6.6831	6.8221	13.1518
$\mu = 0.5, \xi = 0.1$	9.1751	38.5047	0.2177	6.6831	6.9696	11.9395
$\mu = 0.01, \xi = 0.7$	2.52713	44.1045	0.3200	6.6831	6.8135	15.8065
$\mu = 0.5, \xi = 0.2$	11.4335	37.549	0.4668	6.6831	6.7681	12.7518

Table 2 shows the SQM values for the results of the H-ODE model. The results were stable, and the model's performance was good when $\mu = 0.01$ and $\xi = 0.7$,

compared to other values. The H-ODE model will be used to recover the missing region in the structural image component, with parameter values $mu = 0.01$ and $xi = 0.7$, in iteration 900.

4.3. Image inpainting experiments using the NMR algorithm.

The proposed NMR method is applied to restore different-sized lost areas in color image data. Figure 7 displays six inpainting masks that illustrate six damaged regions in images. To evaluate the effectiveness of the proposed method, the NMR method is applied to these masks on 100 images from the Berkeley database.

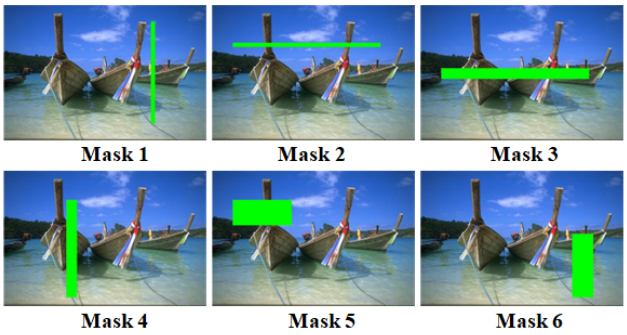


FIGURE 7. The natural color image with different missing areas.

The purpose of using Mask 1 and Mask 2 is to evaluate how well the proposed method can recover texture in small missing regions. In contrast, Masks 3 through 6 are designed to test the method's ability to handle larger damaged areas by utilizing texture information from surrounding regions. Qualitative and quantitative measures were used to evaluate the performance of the NMR technique. Qualitative evaluation focuses on the visual appearance of restored missing areas in images, whereas quantitative evaluation relies on statistical measures, as discussed earlier. Figures 8–13 compare the inpainted images produced by the proposed NMR method with those of two other inpainting approaches: the H-ODE model and the TEBI technique. Figures 8 and 9 show the results of restoring small missing areas in masks 1 and 2. The results shown represent the overall performance observed in most of the images tested.

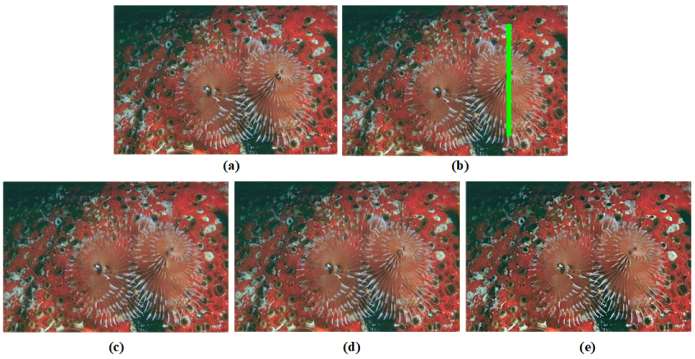


FIGURE 8. Inpainting a Mask 1 image at iteration 500. (a) Reference image, (b) reference image with a mask, (c), (d), and (e) reconstructed images via NMR, H-ODE, and TEBI techniques, respectively.

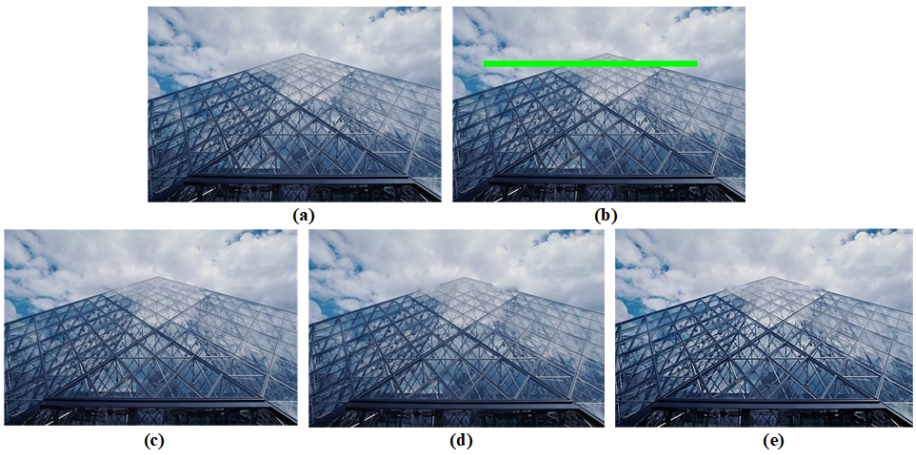


FIGURE 9. Inpainting a Mask 2 image at iteration 500. (a) Reference image, (b) reference image with a mask, (c), (d), and (e) reconstructed images via NMR, H-ODE, and TEBI techniques, respectively.

Figures 10-13 show the results of restoring large missing areas in some standard color images.

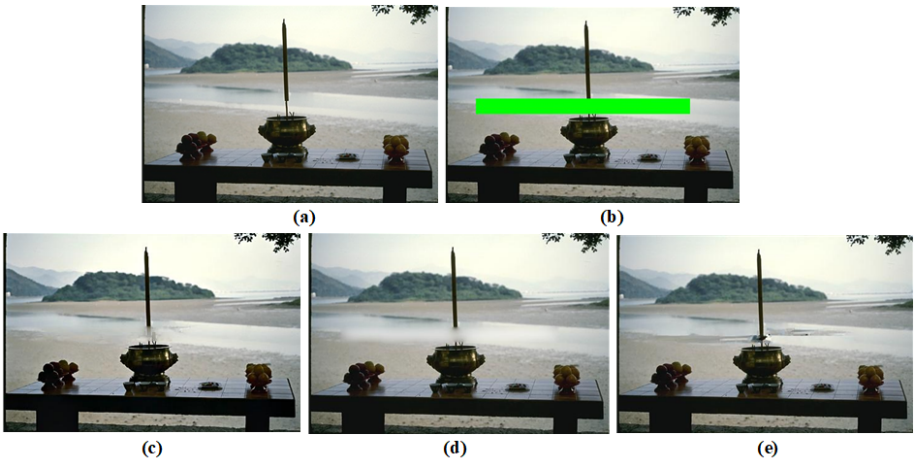


FIGURE 10. Inpainting a Mask 3 image at iteration 900. (a) Reference image, (b) reference image with a mask, (c), (d), and (e) reconstructed images via NMR, H-ODE, and TEBI techniques, respectively.

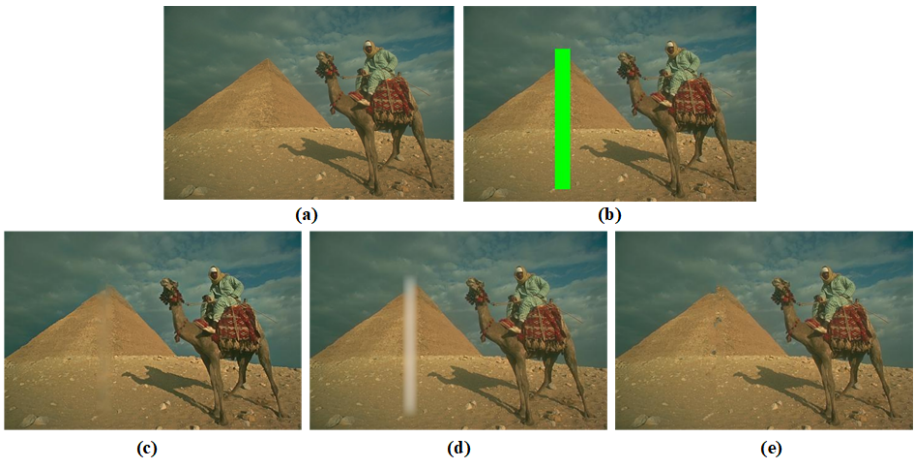


FIGURE 11. Inpainting a Mask 4 image at iteration 900. (a) Reference image, (b) reference image with a mask, (c), (d), and (e) reconstructed images via NMR, H-ODE, and TEBI techniques, respectively.

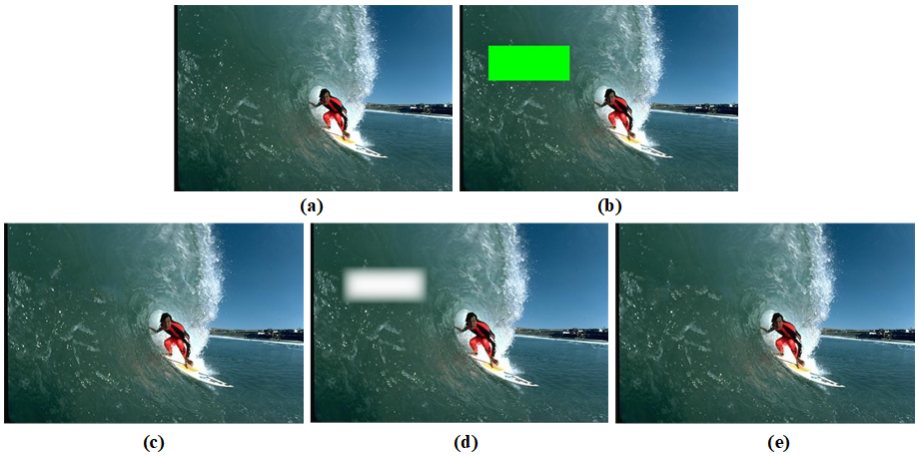


FIGURE 12. Inpainting a Mask 5 image at iteration 1100. (a) Reference image, (b) reference image with a mask, (c), (d), and (e) reconstructed images via NMR, H-ODE, and TEBI techniques, respectively.

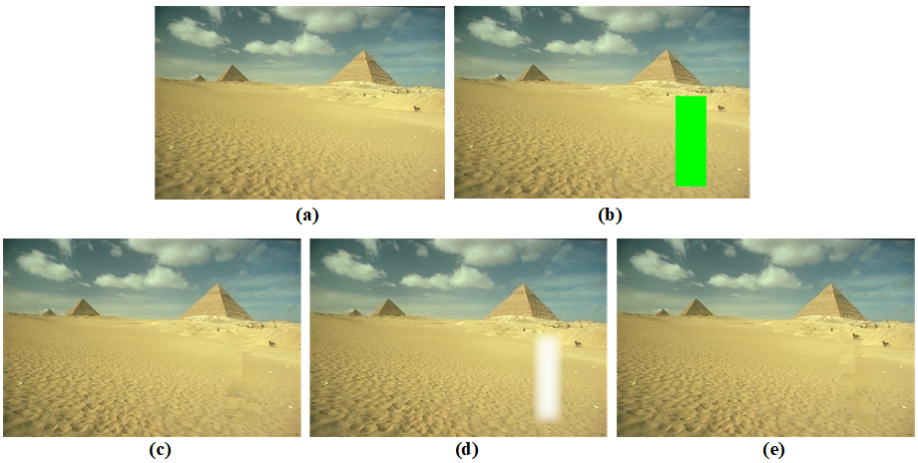


FIGURE 13. Inpainting a Mask 6 image at iteration 1100. (a) Reference image, (b) reference image with a mask, (c), (d), and (e) reconstructed images via NMR, H-ODE, and TEBI techniques, respectively.

As shown in Figures 8–13, the NMR method generally performs better than both the H-ODE model and the TEBI approach. The NMR technique results appear more natural and consistent in visual assessment because this technique preserves structural properties such as curvature and continuity and efficiently transmits information across large areas of missing data without noticeable distortion. However, in some cases, the reconstructed images from all three methods may appear remarkably similar, as observed across these six mask scenarios. Therefore, quantitative evaluation is essential for a clear comparison of their performance. Figures 14–19 present the mean MSE, SSIM, PSNR, and Entropy for 100 images of masks 1-6, facilitating clearer comparisons among the NMR, TEBI, and H-ODE methods across the eight color spaces.

Figures 14–15 show the mean MSE, SSIM, PSNR, and Entropy for 100 images of masks 1 and 2, respectively, facilitating clearer comparisons among the NMR, TEBI, and H-ODE methods by restoring small missing areas in masks 1 and 2 across the eight color spaces. The results shown represent the overall performance observed in most of the images tested.

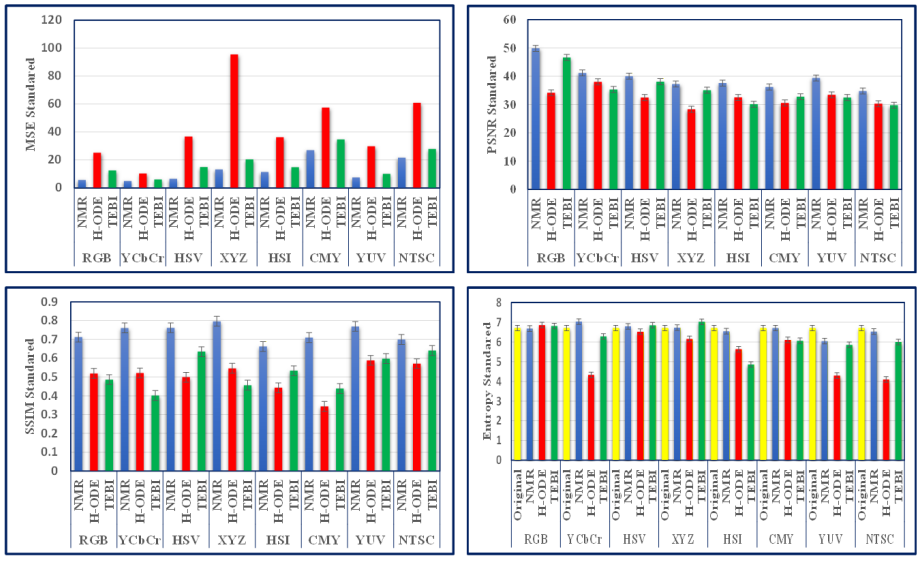


FIGURE 14. The SQMs using NMR, TEBI, and H-ODE techniques for mask 1 in eight color spaces.

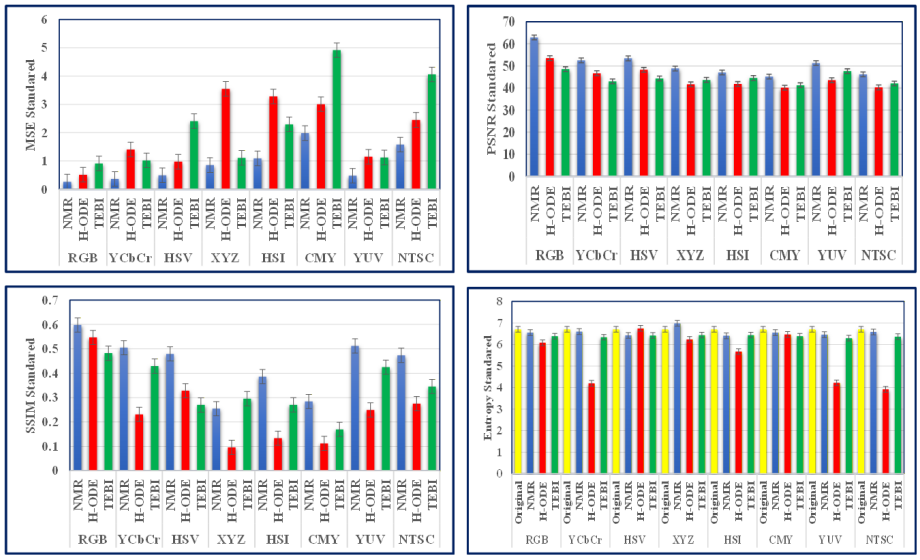


FIGURE 15. The SQMs using NMR, TEBI, and H-ODE techniques for mask 2 in eight color spaces.

Figures 14–15 indicate that the proposed NMR method outperforms both the H-ODE model and the TEBI approach in reconstructing texture and structural details across small missing regions in all eight color spaces. The results show that NMR generally produces higher PSNR, lower MSE, and SSIM values closer to 1, indicating improved reconstruction quality. In addition, the entropy of the images restored with NMR is closer to that of the original images than that of the images restored by the other methods. Figures 14–15 also show results from the suggested NMR technique, which outperforms those from the H-ODE and TEBI methods in recovering texture and structurally damaged regions across all mask images, especially in the RGB, YCbCr, and YUV color spaces.

Figures 16–19 show the mean MSE, SSIM, PSNR, and Entropy for 100 images of masks 3- 6, respectively, facilitating clearer comparisons among the NMR, TEBI, and H-ODE methods by restoring large missing areas in masks 3 - 6 across the eight color spaces.

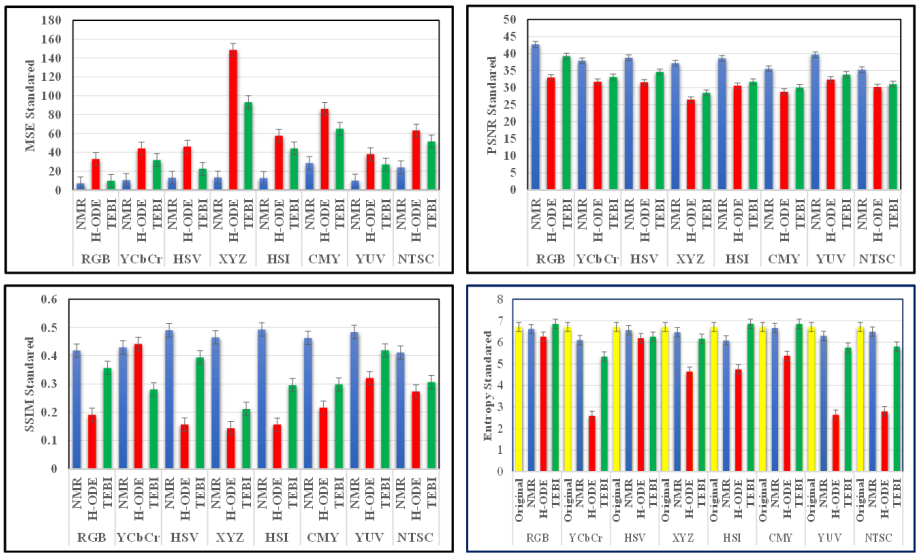


FIGURE 16. The SQMs using NMR, TEBI, and H-ODE techniques for mask 3 in eight color spaces.

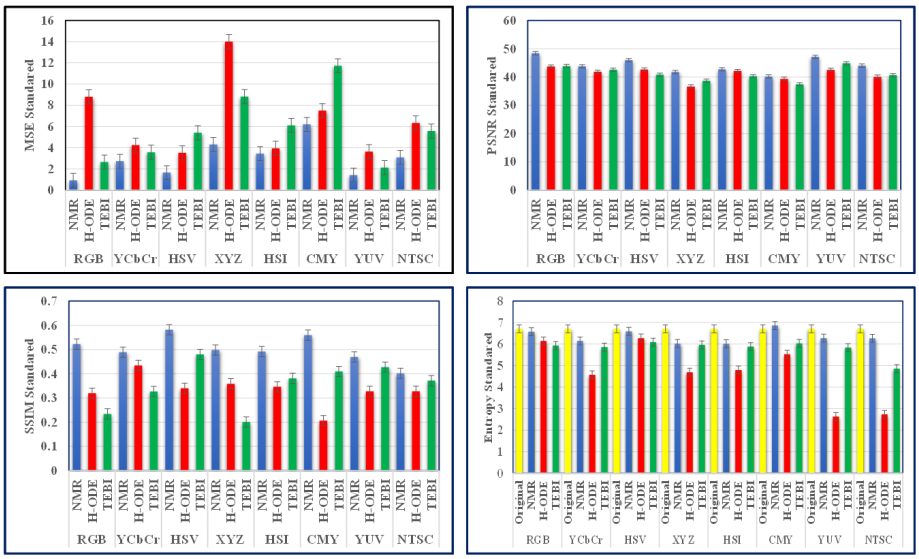


FIGURE 17. The SQMs using NMR, TEBI, and H-ODE techniques for mask 4 in eight color spaces.

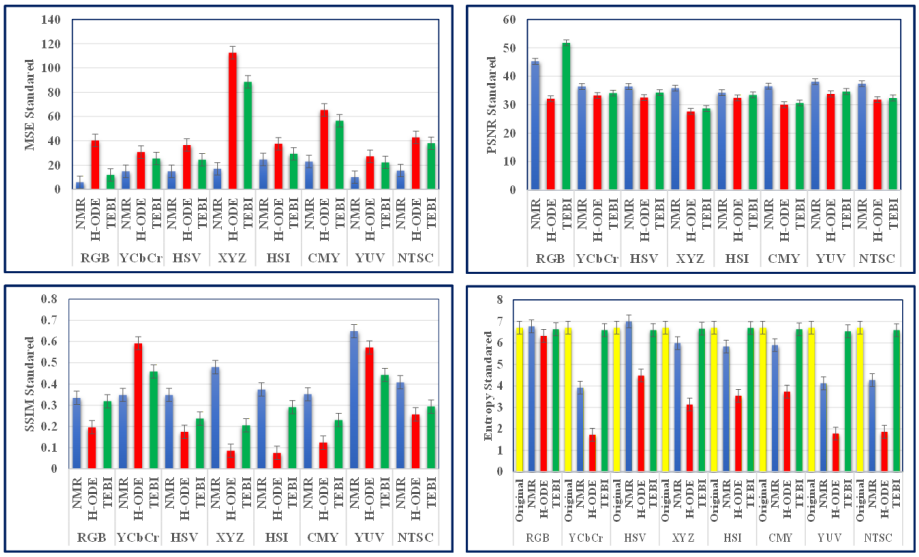


FIGURE 18. The SQMs using NMR, TEBI, and H-ODE techniques for mask 5 in eight color spaces.

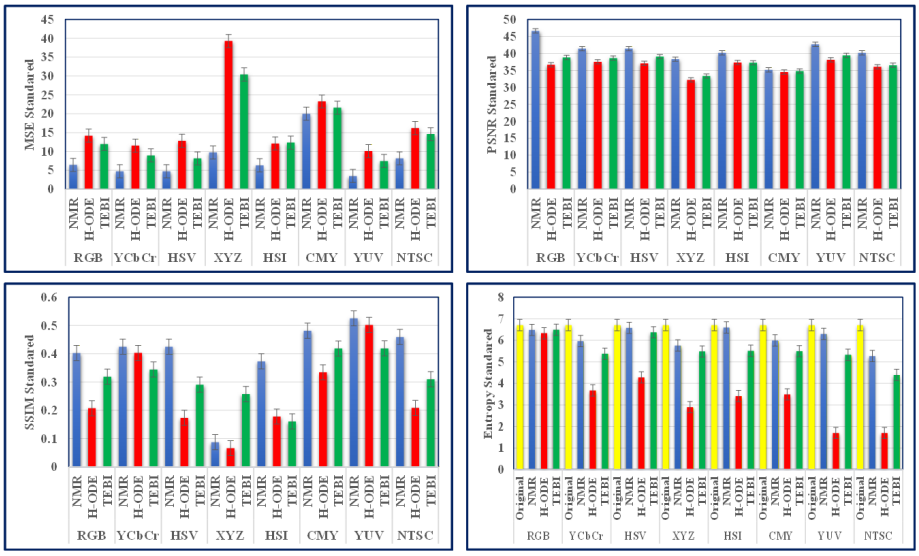


FIGURE 19. The SQMs using NMR, TEBI, and H-ODE techniques for mask 6 in eight color spaces.

Figures 16–19 indicate that the proposed NMR method outperforms both the H-ODE model and the TEBI approach in reconstructing texture and structural details across large missing regions in all eight color spaces. The results show that NMR generally yields higher PSNR, lower MSE, and SSIM values closer to 1, indicating improved reconstruction quality. In addition, the entropy of images restored with NMR is closer to that of the original images than that of images restored by the other methods. Figures 16–19 also show results from the suggested NMR technique, which outperforms those from the H-ODE and TEBI methods in recovering texture and structurally damaged regions across all mask images, especially in the RGB, YCbCr, and YUV color spaces. The NMR approach takes longer to recover large missing regions than H-ODE and TEBI because it integrates three techniques, making it computationally more demanding.

Figures 14–19 indicate that the proposed NMR method consistently outperforms both the H-ODE model and the TEBI approach in reconstructing texture and structural details across different types of missing regions in all eight color spaces. However, this improved performance comes at the cost of increased computational time, as the NMR approach integrates three techniques, making it more computationally intensive than H-ODE and TEBI.

These Figures also show the results obtained using the suggested NMR technique, which outperforms those using the H-ODE and TEBI methods in recovering the texture and structurally damaged regions in the mask 1 image, especially in the YCbCr and YUV color spaces. In the two spaces, the results show SQMs including lower MSE, higher PSNR, and a value of SSIM close to 1, while the value of entropy is closer to the original image entropy value. This improved performance can be attributed to separating the images in the YCbCr and YUV color spaces into the Y (luminance) channel and the (Cb, Cr, U, V) chrominance channels, which help to restore the missing region in mask 1. This separation enables a more effective reconstruction of structure and color information in damaged regions during the inpainting process. The NMR technique takes longer to produce results than other methods because it combines three methods, each of which takes longer to restore damaged areas in the image.

The YCbCr color space is commonly employed in digital image and video compression, whereas YUV has historically been utilized in television broadcasting systems in regions such as Europe and Australia. In both color models, luminance and chrominance are processed separately, which facilitates improved reconstruction compared to color spaces where these components are more closely integrated. This distinction accounts for the greater reliability of YCbCr and YUV in image inpainting tasks.

5. Conclusion and future work

The NMR technique was introduced for simultaneously recovering texture and structural damage regions in an image. This technique combines the MTV,

H-ODE, and TEBI methods. The MTV model was applied to split the image into textural and structural components. The H-ODE method was utilized to restore the damaged area in the structural component image. In contrast, the TEBI method was applied to reconstruct the damaged areas in the textural component image. The NMR technique was utilized to reconstruct six different missing regions in the color image dataset. The NMR method successfully evaluated these missing regions quantitatively and qualitatively across different color spaces. The quantitative metrics for SQMs, including MSE, PSNR, SSIM, and entropy, were applied to evaluate the capacity and efficiency of the NMR technique by applying it to a dataset of natural-color images in eight color spaces. The results demonstrate that the proposed technique outperforms other methods, with lower MSE, higher PSNR and SSIM, and better entropy in each of the eight color spaces. The better results obtained with the NMR technique were in the YCbCr and YUV color spaces across all evaluation SQMs, because these color spaces split the image into a monochrome channel and two chrominance channels, which helps to achieve better performance. However, the NMR method has limitations in recovering high texture in large regions of the image that are missing.

In Future work, we suggest conducting additional studies on this hybrid method and applying it to recover large missing regions in other image datasets, such as medical images, which have important applications in our lives. The NMR technique will also be proposed by combining different ingredients from PDE methods.

Conflicts of interest : The authors declare no conflict of interest.

Data availability: Not applicable

Acknowledgments: The authors are thankful to the reviewers and the editor for their valuable suggestions that improved this work.

References

1. H. Li, L. Hu, J. Liu, J. Zhang, and T. Ma, *A review of advances in image inpainting research*, The Imaging Science Journal **72** (2023), 669-691.
2. M. Bertalmio, G. Sapiro, V. Caselles, and C. Ballester, *Image inpainting*, Proceedings of the 27th annual conference on Computer graphics and interactive techniques - SIGGRAPH '00. ACM Press, **72** 2000, 417-424.
3. M. Benseghir, F.Z. Nouri, and P.C. Tauber, *A new partial differential equation for image inpainting*, B. Soc. Paran. Mat. **39** (2021), 137-155.
4. Seongjai Kim, *PDE-based image restoration: a hybrid model and color image denoising*, IEEE Trans. on Image Process. **15** (2006), 1163-1170.
5. A.A. Efros and T.K. Leung, *Texture synthesis by non-parametric sampling*, in Proceedings of the seventh IEEE international conference on computer vision, IEEE **2** (1999), 1033-1038.
6. A. Criminisi, P. Pérez, and K. Toyama, *Region filling and object removal by exemplar-based image inpainting*, IEEE Transactions on Image Processing **13** (2004), 1200-1212.

7. S. Patil, V.S. Malemath, S. Muddapur, and U.U. Deshpande, *Enhanced Technique for Exemplar-Based Image Inpainting Method*, Advances in Intelligent Systems Research, Atlantis Press International BV (2023), 153-163. doi: 10.2991/978-94-6463-196-8_14.
8. M. Bertalmio, L. Vese, G. Sapiro, and S. Osher, *Simultaneous structure and texture image inpainting*, IEEE transactions on image processing **12** (2003), 882-889.
9. I.J. Sreelakshmy and B.C. Kovoor, *A Hybrid Inpainting Model Combining Diffusion and Enhanced Exemplar Methods*, J. Data and Information Quality **13** (2021), 1-19.
10. Z. Chen, K. Du, Y. Sun, X. Lin, and X. Ma, *Hierarchical neural network for hand pose estimation*, Signal Processing: Image Communication **72** (2020), p. 115909.
11. C.-H. Yeh, H.-F. Yang, M.-J. Chen, and L.-W. Kang, *Image inpainting based on GAN-driven structure- and texture-aware learning with application to object removal*, Applied Soft Computing **161** (2024), p. 111748.
12. D. Pathak, P. Krahenbuhl, J. Donahue, T. Darrell, and A.A. Efros, *Context encoders: Feature learning by inpainting*, In Proceedings of the IEEE conference on computer vision and pattern recognition, 2016, 2536-2544.
13. A. Khan, Z. Rauf, A. Sohail, A.R. Khan, H. Asif, A. Asif, and U. Farooq, *A survey of the vision transformers and their CNN-transformer based variants*, Artificial Intelligence Review **56** (2023), 2917-2970.
14. H. Long, *Hybrid design of CNN and vision transformer: A review*, In Proceedings of the 2024 7th International Conference on Computer Information Science and Artificial Intelligence, 2024, 121-127.
15. Y. Li and G. Wu, *Multi-Scale Feature Fusion and Global Context Modeling for Fine-Grained Remote Sensing Image Segmentation*, Applied Sciences **15** (2025), p. 5542.
16. S. Rawat, A. Srinivasan, V. Ravi, and U. Ghosh, *Intrusion detection systems using classical machine learning techniques vs integrated unsupervised feature learning and deep neural network*, Internet Technology Letters **5** (2022), p. e232.
17. M.R. Hudagi, S. Soma, and R.L. Biradar, *DKH: a hybridized approach for image inpainting using Bayes probabilistic-based image fusion*, International Journal of Intelligent Robotics and Applications **7** (2023), 149-163.
18. H. Qu, L. Ning, R. An, W. Fan, T. Derr, H. Liu, X. Xu, and Q. Li, *A survey of mamba*, arXiv preprint arXiv:2408.01129 (2024). doi: 10.48550/arXiv.2408.01129
19. Y. Huang, J. Huang, J. Liu, M. Yan, Y. Dong, J. Lv, C. Chen, and S. Chen, *Wavedm: Wavelet-based diffusion models for image restoration*, IEEE Transactions on Multimedia **26** (2024), 7058-7073.
20. H. Wang, W. Wang, X. Wang, X. Yuan, and M. Chen, *Frequency-Guided Wavelet Transformer for Effective Moiré Pattern Removal*, Communications in Computer and Information Science, Springer Nature Singapore (2025), 376-387. doi: 10.1007/978-981-96-9949-0_32.
21. D.O. Kolodochka and M.V. Polyakova, *Lama-wavelet: image impainting with high quality of fine details and object edges*, Radio Electronics, Computer Science, Control **1** (2024), p. 208.
22. L. Xiao and J. Wu, *Image inpainting algorithm based on double curvature-driven diffusion model with P-Laplace operator*, PLoS ONE **9** (2024), p. e0305470.
23. S.A. Jassim, A. Al-jaberi, A.T. Asaad, and N. Al-Jawad, *Topological data analysis to improve exemplar-based inpainting*, Mobile Multimedia/Image Processing, Security, and Applications 2018, SPIE (2018), p. 4. doi: 10.1117/12.2309931.
24. L.I. Rudin, S. Osher, and E. Fatemi, *Nonlinear total variation-based noise removal algorithms*, Physica D: Nonlinear Phenomena **60** (1992), 259-268.
25. A.K. Al. Ajberi and Z.R. Jawad, *A Novel Total Variation Model for Image Denoising with Different Types of Noise*, Iraqi Journal of Science **66** (2025), 3907-3920.
26. C. Bazan, M. Abouali, J. Castillo, and P. Blomgren, *Mimetic finite difference methods in image processing*, Computational & Applied Mathematics **30** (2011), 701-720.

27. F. Benzarti and H. Amiri, *Image inpainting via isophotes propagation*, 2012 6th International Conference on Sciences of Electronics, Technologies of Information and Telecommunications (SETIT), Sousse, Tunisia, 2012, 359-364.
28. S. Esedoglu and J. Shen, *Digital inpainting based on the Mumford-Shah-Euler image model*, European Journal of Applied Mathematics **13** (2002), 353-370.
29. S. Karanwal, *Robust local binary pattern for face recognition in different challenges*, Multimed Tools Appl. **81** (2022), 29405-29421.
30. L.-J. Deng, T.-Z. Huang, and X.-L. Zhao, *Exemplar-Based Image Inpainting Using a Modified Priority Definition*, PLoS ONE **10** (2015), p. e0141199.
31. T. Xu, T.-Z. Huang, L.-J. Deng, X.-L. Zhao, and J.-F. Hu, *Exemplar-based image inpainting using adaptive two-stage structure-tensor based priority function and nonlocal filtering*, Journal of Visual Communication and Image Representation **83** (2022), p. 103430.
32. Y. Petcharaporn, P. Kumam, J. Martínez-Moreno, and W. Jirakitpuwapat, *Image inpainting via modified exemplar-based inpainting with two-stage structure tensor and image sparse representation*, Mathematical Methods in the Applied Sciences **47** (2024), 9027-9045.
33. R. Lenka, K. Dutta, S.K. Sarangi, and S. Ramavath, *Improvement of exemplar-based inpainting by enhancement of patch prior*, In 2023 IEEE 3rd International Conference on Applied Electromagnetics, Signal Processing, & Communication (AESPC), IEEE, 2023, 1-4.
34. P. Arbelaez, C. Fowlkes, and D.M. Pablo, *The Berkeley Segmentation Dataset and Benchmark*, 2007. Available: https://www2.eecs.berkeley.edu/Research/Projects/CS/vision /bsds/
35. Y. Yang, Z. Lei, and C. Li, *No-Reference Image Quality Assessment Combining Swin-Transformer and Natural Scene Statistics*, Sensors **24** (2024), p. 5221.
36. Z. Chen, J. Du, J. Li, and H. Lv, *MDFN: Enhancing Power Grid Image Quality Assessment via Multi-Dimension Distortion Feature*, Sensors **25** (2025), p. 3414.
37. Dr. M.R. Raigonda and Shweta, *Signature Verification System Using SSIM In Image Processing*, JSRT (2024), 5-11. doi: 10.61808/jsrt79
38. Y. Li and X. Chao, *Distance-Entropy: An Effective Indicator for Selecting Informative Data*, Front. Plant Sci. **12** (2022). doi: 10.3389/fpls.2021.818895.
39. Y. Wang, and Y.Q. Zhang, *Video processing and communications*, Upper Saddle River, Prentice Hall **1** (2002), 241-248.
40. P. Liu and X. Du, *Research and improvement of the formula of correlation coefficient in image processing*, Electrical Engineering and Computer Science (EECS) **1** (2019), 1-10.

Ahmed K. Al-Jaberi received his M.Sc. degree from the University of Basrah and his Ph.D. degree from the University of Buckingham. He is currently an Assistant Professor at the University of Basrah. His research interests include differential equations, numerical optimization, mathematical computation, and image processing.

Department of Mathematics, College of Education for Pure Science, University of Basrah, Basra, Iraq.
e-mail: ahmed.shanan@uobasrah.edu.iq

Zainab H. Ahmed received her M.Sc. degree from Tikrit University and her Ph.D. degree from the University of Sfax, Tunisia. She is currently an Assistant Professor at Tikrit University. Her research interests include numerical optimization, image processing, and applied mathematics.

Department of Mathematics, College of Science, Tikrit University, Tikrit 34001, Iraq.
e-mail: zahmed@tu.edu.iq

Ali Hasan Ali received his M.Sc. degree from Wright State University, USA, and his Ph.D. degree from the University of Debrecen, Hungary. He is currently an Assistant Professor at

the University of Basrah. His research interests include numerical analysis, applied mathematics and mathematical modeling, computational mathematics, iterative methods, and parallel computing.

Department of Mathematics, College of Education for Pure Science, University of Basrah, Basra, Iraq.
Technical Engineering College, Al-Ayen University, Dhi Qar 64001, Iraq.
e-mail: ali.hasan@uobasrah.edu.iq